High-temperature high-velocity impact on honeycomb sandwich panels

W.H. Xie [a], S.H. Meng [a], L. Ding [b], H. Jin [a], S.Y. Du [a], G.K. Han [a], L.B. Wang [a], C.H. Xu [a], Fabrizio Scarpa [c], R.Q. Chi [d]

[a] Center for Composite Materials and Structures, Harbin Institute of Technology, No.2 Yikuang Street, Harbin 150080, China

[b] Center for Advanced Composite Materials, Shenzhen Academy of Aerospace, Keji South Ten Road 6, Shenzhen, 518057, China

[c] Advanced Composites Centre for Innovation and Science (ACCIS), University of Bristol, BS8 1TR Bristol, UK

[d] Hypervelocity Impact Research Center, Harbin Institute of Technology, No.2Yikuang Street, Harbin 150080, China

Abstract

This work presents an investigation on the damage and high-speed impact deformation mechanisms at elevated temperatures in honeycomb sandwich panels made from PM1000 and PM2000 alloys. The impact temperatures ranged from 22 ℃ to 866 ℃. The investigation was performed experimentally using a custom-made gas gun rig, and by using Finite Element and developing a phenomenological analytical model to predict the residual velocity and ballistic limit equations for the case in which the diameter of the projectile is close or smaller to the honeycomb cell length. The sizes of the holes have been also evaluated by carrying out numerical thermal loading simulations on honeycomb sandwich specimen models impacted at high speed. The predictions provided by the Finite Elements and the analytical model give a good agreement with the results from the experimental tests. The hole diameters for the two idealized normal impact cases, in which the projectile hits the cell core and at the triple-wall intersection of the core, were also presented as a function of the projectile diameter and velocity in this paper.

Keywords:

A. Honeycomb Sandwich; B. Impact behavior; C. High-temperature; D. Failure.

Nomenclature

Parameter	Definition
d_p	Projectile diameter
t_f	Thickness of the front face skin
t_b	Thickness of the back face skin
t_c	Thickness of the honeycomb core
V_0	Impact velocity [km/s]
θ	Impact angle
T	Test temperature
A_{front}	Area of the damage hole at the front side of the specimen face skin
A_{back}	Area of the damage hole at the back side of the specimen face skin
V_p	Normal impact velocity of the projectile [km/s]
V_f	Residual velocity of the projectile [km/s]
m_p	Mass of projectile
m_b	Mass of the plug moved out from the honeycomb sandwich panel
W_f	Kinetic energy lost due to the inelastic impact of the projectile on the plug free of the surrounding material
W_s	Energy lost during the penetration
W_{sf}	Energy lost during the penetrations of the front face skin
W_{sc}	Energy lost during the penetrations of the honeycomb core
W_{sb}	Energy lost during the penetrations of the back face skin
d_f	Hole diameter of the front face skin
d_b	Hole diameters of the back face skin
d_h	Hole diameter of the normal impact
σ_f	Dynamic yield shear strength of the front face skin
σ_b	Dynamic yield shear strength of the back face skin
x	Forward distance along the direction of velocity
d_{pc}	Critical diameter of the projectile for ballistic limit impact
ρ_p	Density of the projectile
ρ_f	Density of the front face skin
ρ_b	Density of the back face skin
$d_{h\theta}$	Actual hole diameter of the oblique impact experiments

1. Introduction

Honeycomb sandwich structure have a very low weight and feature high stiffness, and durability. Honeycombs with hexagonal cells are the most common structures among cellular materials, although the shape of honeycomb cells had evolved from hexagonal to square, triangular [1], columnar [2] or other related shapes [3-6].

The in-plane mechanical behavior of regular hexagonal honeycombs has been extensively investigated in a large number of research papers [7-10]. The majority of the existing analytical studies tend to simulate the mechanics of honeycomb structures as a 2D problem. For example, Zhu and Mills [9] have theoretically analyzed in-plane uniaxial compression of regular honeycombs, while Fleck and Qiu have developed an approach to predict the fracture response of elastic-brittle 2D lattices [8]. The out of plane mechanical behavior of honeycombs were mainly studied by impact test and simulation analysis. Most researchers have been devoted to the study of low-velocity impact of aluminum honeycomb panels. For example, Vaziri et al.[11] illustrated a finite element method to evaluate the structural response and failure modes of honeycomb sandwich panels. Wang et al.[12] have focused on the dynamic impact response of aluminum honeycomb panels under axial impact. Fei et al.[13] and Nia et al.[14] carried out experimental investigation on the surface deformation and damaged zone of panels at low-velocity impact.

In addition to the metallic honeycomb, many researchers have also devoted a significant effort to describe the impact on composite-metal hybrid sandwich structures. Ryan A et al. [15-17] have described a number of common approaches to predict the ballistic limit of CFRP/Al honeycomb sandwich panels using impact test data. G. Morada et al.[18] and W. He et al.[19] performed a series of low-velocity impact tests to investigate the impact properties of combined

composite-metal hybrid structures. Feli et al. [20] and Barbero et al. [21] have introduced the analytical models and a three dimensional finite element model to investigate the perforation resistance of composite-metal hybrid sandwich panels subjected to high-velocity impact.

In addition to the sandwich structure, experimental and computational methods have also been developed to better understand the impact response in simpler composite laminates and metallic plates. Sarasini et al.[22-24], Zouggar et al.[25], Bandaru et al.[26] , Zhang et al.[27], M. Landowski et al. [28] and M. Ravandi et al. [29] focused their efforts on composite laminates, and provided some useful simulation and experimental methods for low-velocity impact (<1 km/s). while most of the studies of the impact of the metallic plate were aimed at the high-velocity impact of aluminum plate. Piekutowski et al. [30, 31] have investigated the penetration, projectile fragmentation and debris cloud of high velocity impacts, and a series of theoretical ballistic limit equations for aluminum plates were developed by Christiansen et al. [32, 33] and his group.

Although some quite useful design guidelines can be derived from the previous works and data are available about impact tests carried out between room temperature and 300 ℃[34-36], high-velocity impact tests on honeycomb sandwich structures at high temperatures are still scarce. This is due to the limitation of the temperature resistance of the materials studied and the significant costs associated to these experiments[37-40].

This paper presents an experimental, numerical and analytical investigation about the effects of high velocity impacts (200 ms^{-1}-3500 ms^{-1}) and the related damage on honeycomb sandwich panels with superalloy PM1000 and PM2000 cores at high temperatures (between 22 ℃ and 866 ℃). The temperatures have been reached by using a fast electric heating system. The high-

speed impact experimental tests at high-temperature have been performed using a custom-made facility that will be described in detail in the following paragraphs. An analytical model describing the impact on honeycomb sandwich panels to obtain the residual velocity and the ballistic limit equations has been also developed. The model relates the hole diameter of the honeycomb sandwich panel with the dynamic yield strength at high temperatures, together with its impact speed and the dimensions of the facing skins. The hole diameter must be assigned to obtain the residual velocity and the ballistic limit curves in the presented model. For the two idealized normal impact cases in which the projectile hits the cell core and at the triple-wall intersection of the core, the hole diameters were presented as a function of the projectile diameter and velocity in this paper. The focus of this paper is also about oblique high-speed impacts, which tend to represent some realistic impact situations, in particular for what it concerns space debris. There is scarcity of data about oblique impacts at high speed in honeycomb sandwich panels, especially at high temperatures (higher than 800 ^{o}C) [41-43]. With the present work we also aim at generating more experimental and simulations data in this particular topic, and providing formulas to be used for design guidelines for airframe and spacecraft applications.

2. High-Temperature Impact Experimental Tests

2.1 Design of the High-Temperature Impact Facilities and Test Procedure

The impact facilities shown in Fig. 1 and Fig. 2 [44] consist of a two-stage light-gas gun and a fast electric heating system. The two-stage light-gas gun has been used to accelerate spherical projectiles. The fast electric heating system consisted of two copper (Cu) electrodes, a cool water device and voltage transformer. The custom heating system could be used to heat the specimens

and also measure the temperatures of the specimens. During each test the specimen was connected to the two Cu electrodes, which were then fixed in a supporting back plate (Fig. 1 (b)). The temperature of the specimen could be controlled through a variable current with an adjustable range between 10A and 5000A. The voltage at the two ends of the specimen was maintained at 1V~4 V, and the current adjusted by software. The temperatures of the specimens were measured using a multi-wavelength pyrometer with a measurement range of 350 ℃~3000 ℃.

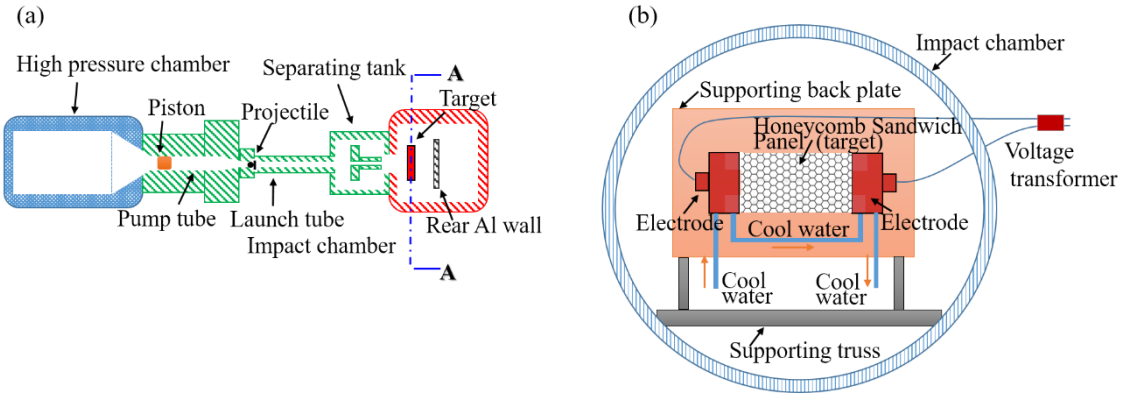

Fig. 1.Schematics of the impact facilities: (a) Two-stage light gas gun; (b) Impact setup in light gas gun impact chamber

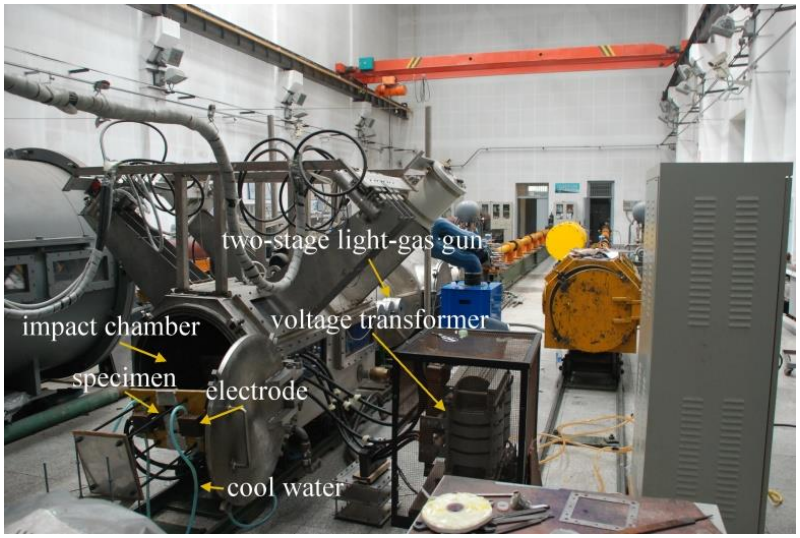

Fig. 2.Impact test setup (From[44])

The ballistic performance of honeycomb sandwich specimens was investigated by oblique impact with velocities of 2.476 km/s, 2.411 km/s, 3.5 km/s and 3.258km/s. Fig. 3 shows a typical

sketch of the impacts. For the specimen used in this paper, $t_f = t_b$ =0.125mm and t_c =3.5mm. The impact angles θ were 45 ° and 30 °. The impact test temperatures of the specimens were 442 ℃, 866 ℃, 839 ℃ and 465 ℃.

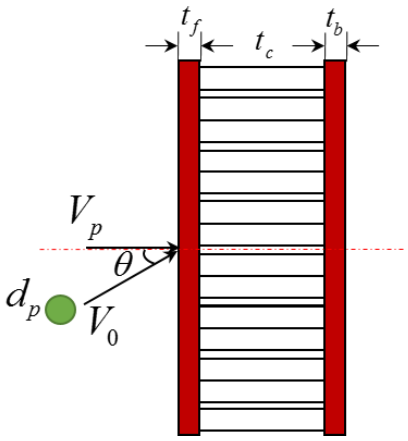

Fig. 3 . Schematics of the impact on a honeycomb sandwich panel

In all cases, 3mm diameter spheres made from Si_3N_4 impacted the specimens. The sizes of the specimens are shown in Fig. 4. The front and back face skins were made of PM2000 and PM1000. The honeycomb core material was PM1000, and the single wall thickness of the honeycomb cell was 0.125mm. The core was produced by classical gearing forming of corrugated ribbons, which were connected together through manual spot welding. Brazing in vacuum then assembled the plates and the core.

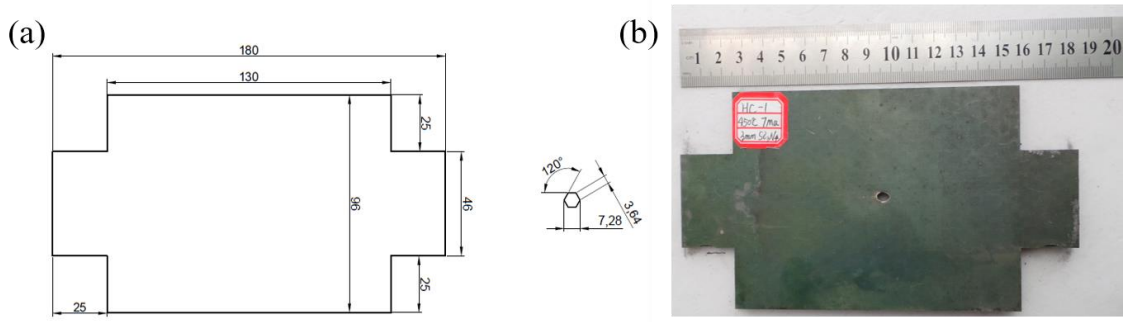

Fig. 4 Honeycomb sandwich specimens (unit: mm) (a) Dimension (b) Photo after impact

2.2 Impact Test Results

During the test campaign four experiments were performed. After the impact tests the states of the damage on the front and back sandwich skins of the specimens were observed and quantified by measuring the perforated hole-areas of the front and back facing skins. Table 1 presents a summary of the impact test results. The back face sheets of the perforated honeycomb sandwich specimens are damaged over a broader surface, larger (between 3.5 and 7 times) than the damaged one of the front face skins.

Table 1 Impact test results

NO.	V_0（km/s）	θ（°）	T（℃）	Test result	Damage area（mm^2）	
					A_{front}	A_{back}
HC-1	2.476	45	442	Perforated	18.7	124.6
HC-2	2.411	30	866	Perforated	14.4	49.9
HC-3	3.500	45	839	Perforated	19.5	111.3
HC-4	3.258	30	465	Perforated	14.7	52.4

The damages of the honeycomb sandwich panels were shown in Fig. 8~Fig. 15, which were presented in Section 3.2 for convenient comparison between the FE and the experimental results.

During the HC-1 test the projectile hit the specimen at an impact angle of 45º, with a velocity of 2.476km/s at a temperature of 442 ºC. The shape of the perforation on the front face skin of the specimen was elliptical, and there was no obvious presence of wrinkles and hollowing out in the area around the hole. The back face skin of the perforation was petal shaped, and a large area damage was caused by the large angle oblique impact. This large damage section also led to the loss of the core around the perforation. Although the HC-3 test was different from the HC-1 one in terms of velocity and temperature, the impact angles of the two tests were the same. The shapes of the damage created in the two tests were similar: the perforation in the front face skin was

elliptic and the damage area in the back face skin was relatively large, leading to core loss.

During the HC-2 test the projectile hit the specimen at an impact angle of 30º. The velocity of the projectile was 2.411km/s, and the test was carried out at 866 ºC. In the front face skin a perforation was formed with the shape of an ellipse, closer to a circle. Also in this case, no obvious wrinkling and hollowing out in the area around the hole were present. On the back face skin an irregular perforation was observed, and the damage area was significantly reduced compared to the one present in the HC-1 test. The experimental results show that the impact angle has a significant influence on the damage area. The results from the HC-4 tests were similar to those of HC-2.

In summary, the shapes of the holes in the front skins were all elliptical, while those of the back skins had an irregular contour. The shapes of the perforations tended to be close to circles at lower impact angles, a fact that agrees well with the shapes of the holes being circular as observed in normal impact [45].

3. High-Temperature Impact Numerical Tests

3.1 Numerical model

Fig. 5 shows the Finite Element model used in this work. The material properties of the PM1000, PM2000 alloys and Si_3N_4 used in the FE model are shown in Table 2. All the simulations have been carried out using the Explicit Dynamics module in ANSYS WORKBENCH (Version 16.1), which is more convenient for engineering simulations than classic ANSYS. The calculations were performed on a Windows-based machine with 4.8GHz CPU and 32GB RAM. SHELL181 elements and a linear elastic constitutive model with large geometric deformations

have been used to represent both the core and the face skins (Fig. 6). Since the spherical projectiles used during all the four tests exhibited no visible deformation, the finite element model representing the projectiles was a rigid one. The SOLID185 element was used for the projectile. The linear triangular elements of Conta173 and Targe170 were used for the honeycomb sandwich panels and the rigid projectile respectively. The contact body interaction geometry was set as "all bodies" and the auto detection of generating automatic connection on refresh was turned on. The element degrees of freedom concluded the displacement (UX, UY, UZ) and temperature (TEMP). The contact type was frictionless. The maximum offset was $10^{-7}m$.

The type of analysis was set as "high velocity". After defining the engineering material properties for PM1000 and PM2000, given in Table2, the tensile strength at different temperatures were used as the material failure criteria. Then the erosion control was set as "on material failure". The inertia of eroded material was retained. The 3D model has been produced in SOLIDWORKS (Version 2014), and then imported into the ANSYS WORKBENCH platform. The minimum and maximum edge length of each element were set at 0.003mm and 0.5mm, respectively. The number of elements used for each model was above 200000. Because the specimens during each test were impacted after heating to a maximum temperature, the numerical model represents first a static thermal pre-stress problem. Transient heating and large deformations during the static thermal simulations were not considered because the electric heating support part in the experiment could be removed to release the thermal deformation, therefore making the use of large displacements during the FE simulations not necessary.

To simulate the boundary of the specimen during the tests, one side of the model was fixed

in all directions, while the other side was fixed along the normal direction only. Because the impact position cannot be obtained through the impact experiments, during the simulations the projectile was moved at small steps to adjust the initial impact position and make sure that the simulation results were coincident with the experimental ones. Fig. 8~Fig. 15 show the relative position between the damage hole and the honeycomb core. One can observe that the initial impact position in each simulation is consistent with the experimental findings.

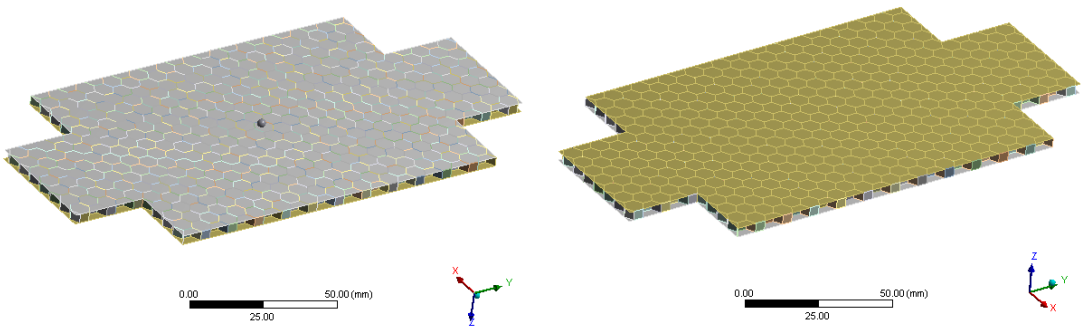

Fig. 5 Numerical model

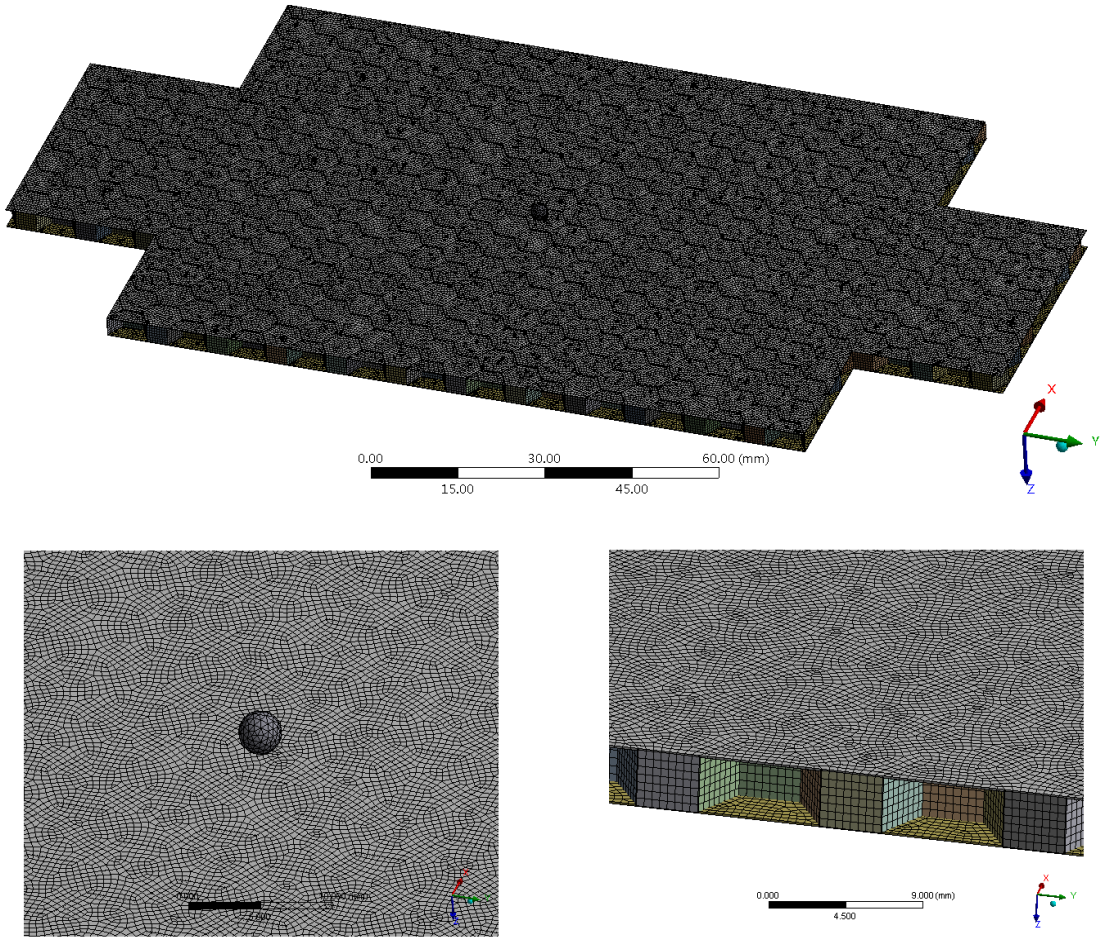

Fig. 6 Ensemble view and details of the explicit Finite Element models used in the simulations

Table 2 Material properties of simulations[46, 47]

Material	**PM1000**			**PM2000**			**Si_3N_4**
Temperature	22 ℃	400-500 ℃	800 ℃-900 ℃	22 ℃	400-500 ℃	800-900 ℃	22 ℃-900 ℃
Density (g/cm^3)	8.24	8.24	3.31	7.18	7.18	7.18	3.31
Elastic modulus (GPa)	210	210	210	157	157	157	
Tensile strength (MPa)	922	796	238	618	131	91	

3.2 Comparison between the FE and the experimental results

Table 3 shows the comparison of the damage areas simulated by the numerical models, and the experimental results.

Fig. 7 shows a typical stress distribution at the contact time for HC-4. It can be seen that at

the contact time, if the element stress exceeds the tensile strength, the element will be eroded and be retained as red erosion points, shown in Fig. 7 (b).

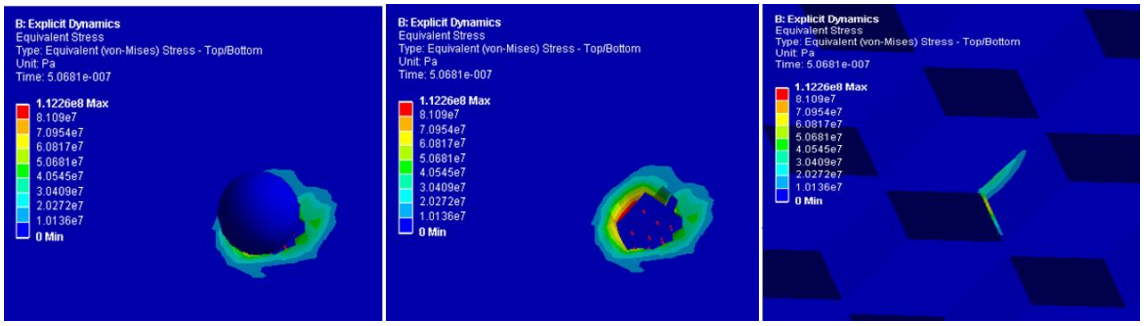

(a) rigid ball (b) the front face (c) the core and back face

Fig. 7 Stress distribution at the contact time

Fig. 8-Fig. 11 show the impact responses obtained by the experimental and numerical methods.

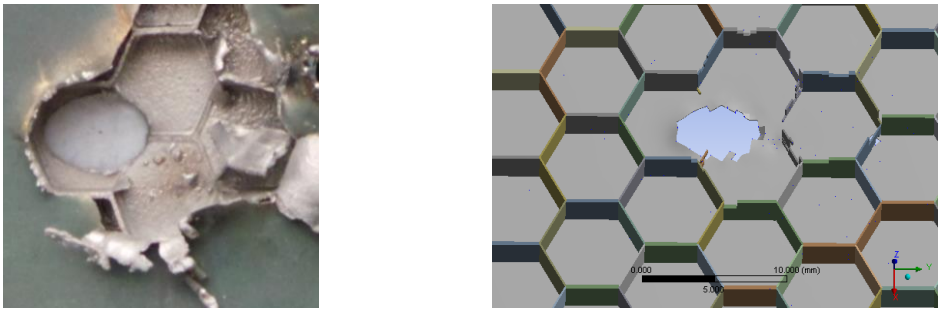

（a）Experimental result （b）Numerical result

Fig. 8 HC-1

（a）Experimental result （b）Numerical result

Fig. 9 HC-2

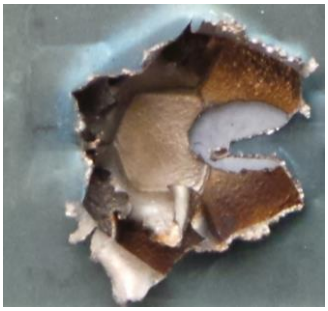

（a）Experimental result

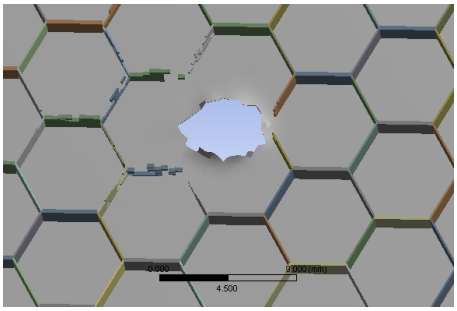

（b）Numerical result

Fig. 10 HC-3

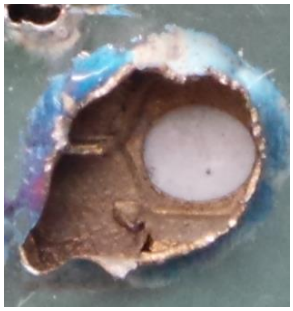

（a）Experimental result

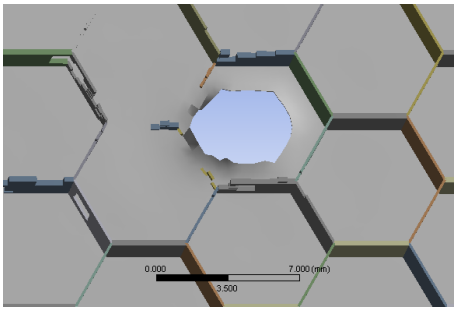

（b）Numerical result

Fig. 11 HC-4

The discrepancies between the predicted and experimental dimensions of the areas are quite contained, with errors ranging between 3.1% and ~ 10%. These results show the remarkable fidelity of the numerical model used. The agreement between the numerical and experimental results indicated that the deformation and stress caused by the removable support during the high temperatures environment tests can be ignored, simply by considering the material strength at those temperatures.

Table 3 Comparison of the damage area of facing skin

NO.	Damage area from experiments（mm²）		Damage area from simulation（mm²）		Err. （%）	
	front	back	front	back	front	back
HC-1	18.7	124.6	18.0	120.7	3.8	3.1
HC-2	14.4	49.9	13.4	54.8	6.5	9.8
HC-3	19.5	111.3	18.3	101.5	6.1	8.8
HC-4	14.7	52.4	13.9	56.6	5.1	8.0

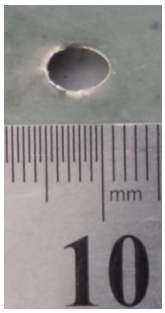

(a) Experimental result of the front face skin

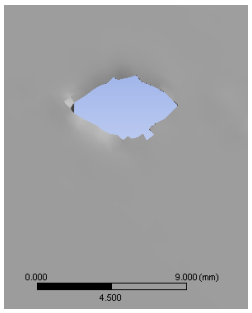

(b) Numerical result of the front face skin

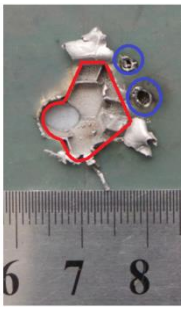

(c) Experimental result of the back face skin

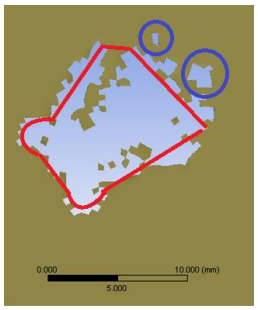

(d) Numerical result of the back face skin

Fig. 12 Numerical and experimental results of the front and back face skins - test HC-1

(a) Experiamental result of the front face sheet

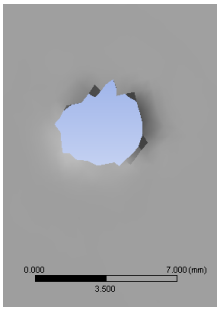

(b) Numerical result of the front face sheet

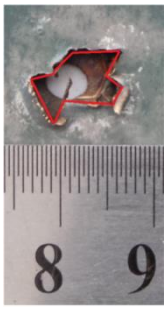

(c) Experiamental result of the back face sheet

(d) Numerical result of the back face sheet

Fig. 13 Numerical and experimental results of the front and back face skins - test HC-2

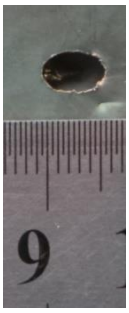

(a) Experimental result of the front face skin

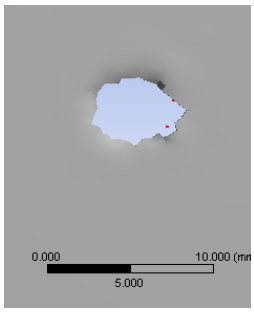

(b) Numerical result of the front face skin

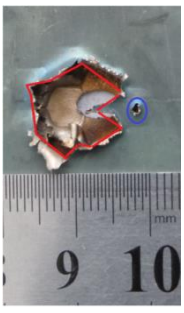

(c) Experimental result of the back face skin

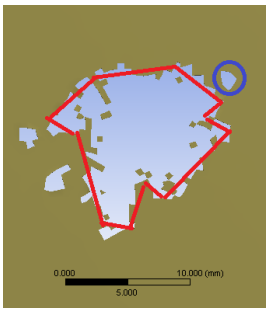

(d) Numerical result of the back face skin

Fig. 14 Numerical and experimental results of the front and back face skin - test HC-3

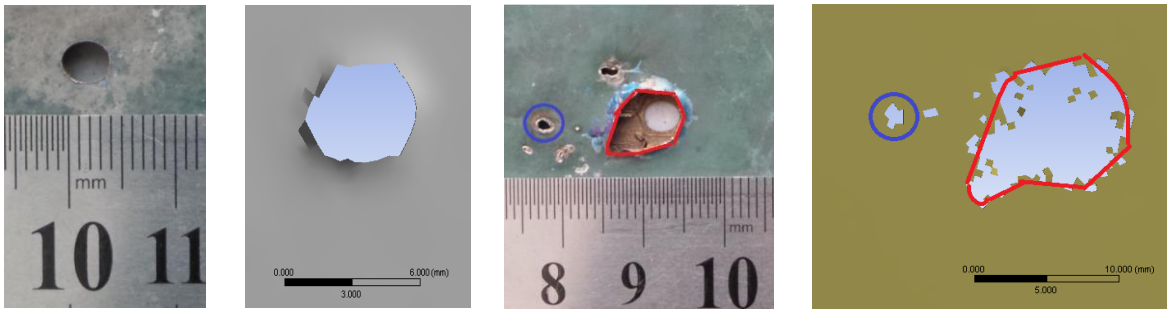

(a) Experimental result of the front face skin

(b) Numerical result of the front face skin

(c) Experimental result of the back face skin

(d) Numerical result of the back face skin

Fig. 15 Numerical and experimental results of the front and back face skin - test HC-4

4. Analytical Model

In open literature several works report the appearance of three distinct velocity regimes that occur during the impact of metal specimens [32, 33, 48, 49]. The first is typical of small impact velocities, with the perforation being dominated by the petalling of the target. The second regime is characterized by the perforation mechanism of the target, which changes from one dominated by petalling to another characterized by a conically shaped plug formation. The third regime is typified by the formation of shaped plugs that cause compression/shear failure in the target. In our tests the projectiles were intact after the impact. The perforation mechanism at high temperature of the front surfaces and on the honeycomb walls appeared to be dominated by shaped plug formation, and a compression/shear failure could be observed. For the back surfaces of the samples some petalling was observed, but the majority of the perforation edges was smooth and dominated by shaped plug formation; the lower the impact angle, the smoother the edges. For the normal impact velocity regime (θ =0) of the reference test (room temperature) the progress of the perforation can be represented as a plug being removed from the honeycomb panel.

In this part, we developed a model to analyze the residual velocity by simplified the energy

balance law for the progression of the perforation produced by a pristine spherical projectile normal impacting on a honeycomb sandwich panel as the removal of a plug by considering the effect of shearing forces and ignoring the energy lost during the local penetration of the honeycomb core. The model is valid for cases in which the projectile diameter is similar or smaller to the honeycomb cell length. By defining the ballistic limit state as the zero residual velocity, a ballistic limit equation for spherical projectiles was also obtained in this part.

If one considers the progression of the perforation produced by a pristine projectile normal impacting on a honeycomb sandwich panel as the removal of a plug (governed by an energy balance law) one obtains:

$$m_p V_p^2 / 2 = \left(m_p + m_b \right) V_f^2 / 2 + W_s + W_f \tag{1}$$

The energy W_s lost during the penetration can be expressed as:

$$W_s = W_{sf} + W_{sb} + W_{sc} \tag{2}$$

For simplification, it can be assumed that the resistance acting on the total mass of the projectile and the plug when they move forward relative to the surrounding materials is mainly provided by shearing forces [50, 51]. Since the energy lost W_{sc} for local shearing cases can be ignored [52], then W_s assumes the following expression:

$$W_s = W_{sf} + W_{sb} \tag{3}$$

For the case of a projectile that normal impact perpendicularly a honeycomb sandwich panel, W_{sf} and W_{sb} can be estimated by:

$$W_{sf} = \int_0^{t_f} \sigma_f \pi d_f \left(t_f - x \right) dx = \sigma_f \pi d_f t_f^2 / 2 \tag{4}$$

$$W_{sb} = \int_0^{t_b} \sigma_b \pi d_b \left(t_b - x\right) dx = \sigma_b \pi d_b t_b^2 / 2 \tag{5}$$

The energy W_f can be estimated directly by momentum and energy considerations [9], i.e. $W_f = m_p m_b V_p^{\ 2} / 2\left(m_p + m_b\right)$. Then Eq.(1) becomes:

$$\frac{m_p V_p^2}{2} = \frac{\left(m_p + m_b\right) V_f^2}{2} + \left(\frac{\sigma_f \pi d_f t_f^2}{2} + \frac{\sigma_b \pi d_b t_b^2}{2} \right) + \frac{m_p m_b V_p^{\ 2}}{2\left(m_p + m_b\right)} \tag{6}$$

The residual velocity V_f can be therefore expressed as:

$$V_f = \left[\frac{m_p^{\ 2} V_p^2}{\left(m_p + m_b\right)^2} - \frac{\sigma_f \pi d_f t_f^2 + \sigma_b \pi d_b t_b^2}{m_p + m_b} \right]^{\frac{1}{2}} \tag{7}$$

To simplify Eq. (7) for cases in which the projectile diameter is similar or smaller to the honeycomb cell length and the perforation mechanism is dominated by the formation of shaped plugs it is assumed that $d_b = d_f = d_h$ (for normal impacts). The residual velocity therefore becomes:

$$V_f = \left[\frac{m_p^{\ 2}}{\left(m_p + m_b\right)^2} V_p^2 - \frac{\sigma_f \pi d_h t_f^2 + \sigma_b \pi d_h t_b^2}{m_p + m_b} \right]^{\frac{1}{2}} \tag{8}$$

For the cases of sphere projectiles we have $m_b = \pi\left(t_f \rho_f + t_b \rho_b\right) d_h^{\ 2} / 4$ and $m_p = \pi d_p^{\ 3} \rho_p / 6$. Introducing these two expressions in into Eq.(8) the residual velocity is equal to:

$$V_f = \left[\frac{d_p^{\ 6} \rho_p^{\ 2} V_p^2}{\left(d_p^{\ 3} \rho_p + 1.5\left(t_f \rho_f + t_b \rho_b\right) d_h^{\ 2}\right)^2} - \frac{6\sigma_f d_h t_f^2 + 6\sigma_b d_h t_b^2}{d_p^{\ 3} \rho_p + 1.5\left(t_f \rho_f + t_b \rho_b\right) d_h^{\ 2}} \right]^{\frac{1}{2}} \tag{9}$$

For the ballistic limit cases (V_f=0)we have the ballistic limit equation for spherical projectiles:

$$d_{pc}^{\ 6} \rho_p^{\ 2} V_p^2 = 6 d_h \left(\sigma_f t_f^2 + \sigma_b t_b^2\right)\left(d_{pc}^{\ 3} \rho_p + 1.5\left(t_f \rho_f + t_b \rho_b\right) d_h^{\ 2}\right) \tag{10}$$

In Eqs.(8) and (10) the diameter d_h should be applied to calculate the residual velocity V_f and obtain the ballistic limit curve.

5. Predictions and Tests

5.1 Prediction and Numerical Test

To obtain a value for the term d_h further impact simulations have been carried out following the methodology describe in Section 3.1. Fig. 16 shows the impact locations in the cases of normal impact for diameters of the projectile similar or smaller to the length of the honeycomb cell. The idealized normal impact cases represent events in which the projectile hits the cell core (IL1) and at the triple-point wall intersection of the core (IL2).

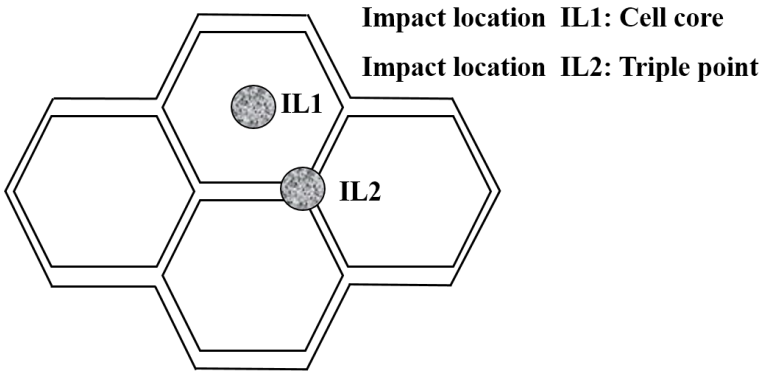

Fig. 16 Honeycomb cell impact location

Forty-three normal impact numerical tests of the cases described above have been performed. The impact velocity ranged from 0.2km/s to 3.5km/s, while the temperature oscillated between 22°C and 800°C. After a regression analysis the values of d_h for the IL1 and IL2 cases can be expressed as exponential functions of d_p and V_p. The following equations can be obtained by fitting forty-three simulation results:

$$d_h = \begin{cases} 2.9619 d_p^{\,1.1637} V_p^{\,0.0393} & for\ IL1 \quad \left(R^2 = 0.9005\right) \\ 2.1835 d_p^{\,1.2369} V_p^{\,0.1256} & for\ IL2 \quad \left(R^2 = 0.9009\right) \end{cases} \tag{11}$$

Fig. 17 and Fig. 18 show the comparison between the residual velocity predicted by Eq.(9) (In which d_h was calculated from Eq.(11)) and the FE simulations. There is a general agreement between the predictions and the Finite Element simulations, especially for the cases in which the impact velocity is lower than 1.5km/s. This might indicate that the part of the energy absorbed by the honeycomb core is negligible in those particular situations. The gap between the simulated results and the analytical predictions increases with the impact velocity, which might indicate that when the impact velocity increases to a certain value the energy absorbed by the honeycomb core could not be neglected anymore. When the speed is higher than 1.5km/s the theoretical calculation results related to the IL2 case are more consistent with the simulation results. that shows that the cell wall directly affects the impact resistance of the structure. The IL2 case can be therefore considered as being more representative of the actual performance of this honeycomb structure. Numerical discrepancies related to the effective hit location and impact angles may have also affected the results, and the theoretical assumption that d_b=d_f may be not completely validated.

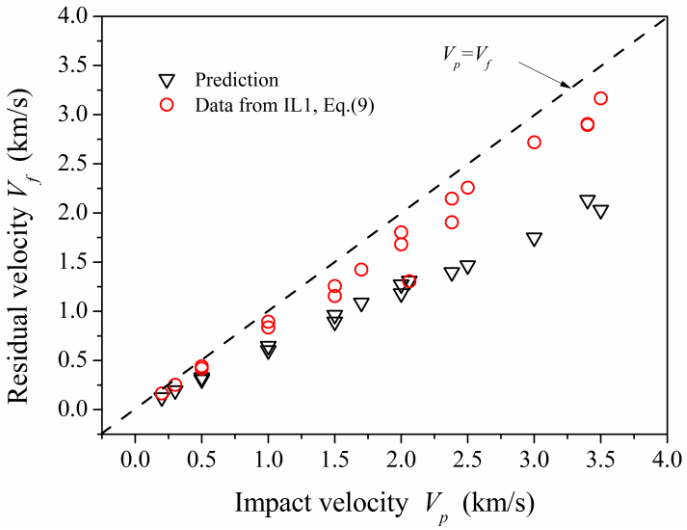

Fig. 17 Comparison between the different sets of results for the IL1 case.

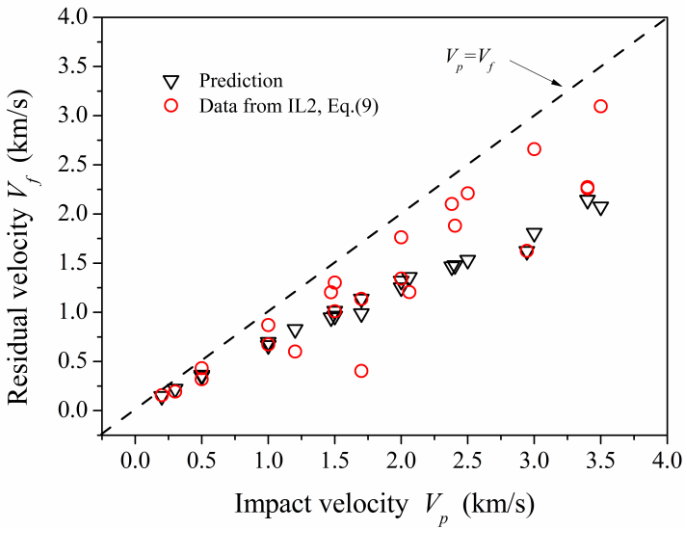

Fig. 18 Comparison between the different sets of results for the IL2 case

5.2 Ballistic limit prediction of experimental test

Since the evidence that the effect of the normal component of the impact velocity provides the most significant contribution to the impact deformation mechanism, it is usual practice to replace the term V_p with the term $V_0\cos\theta$ for the cases of oblique impacts [53]. In this particular case Eq. (10) yields:

$$d_{pc}^{\,6}\rho_p^{\,2}\left(V_0\cos\theta\right)^2 = 6d_{h\theta}\left(\sigma_f t_f^2+\sigma_b t_b^2\right)\left(d_{pc}^{\,3}\rho_p+1.5\left(t_f\rho_f+t_b\rho_b\right)d_{h\theta}^{\,2}\right) \tag{12}$$

The actual hole diameter of oblique impact $d_{h\theta}$ can be calculated as:

$$d_{h\theta}=2\left(A_{front}/\pi\right)^{0.5} \tag{13}$$

The various diagrams in Fig. 19 show the ballistic limit curves of the experimental results obtained from Eq.(12). It can be observed that all the experimental data are well above the ballistic limit curves. The diameter of the projectile used in this work at the current impact velocity is much larger than the critical size, which means that the honeycomb sandwich panel must be perforated - as it happened during the experimental cases. To some extent, these results prove the correctness of our ballistic limit equation. The comparison between the theoretical and the

experimental results shows that the ballistic limit equation can be used to predict the general impact resistance of honeycomb sandwich structures.

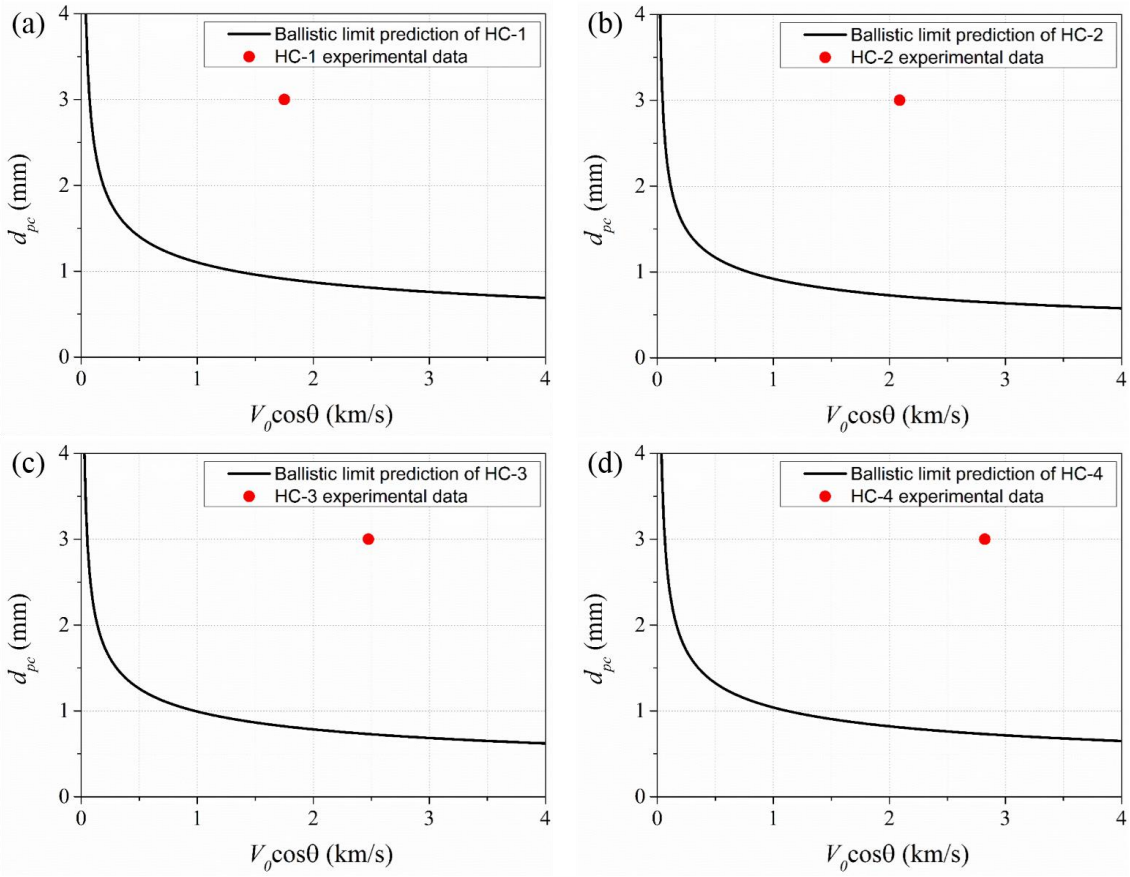

Fig. 19 Ballistic limit predictions and real perforation data for the cases (a) HC-1, (b) HC-2, (c) HC-3 and (d) HC-4

6. Conclusions

This paper has described the high velocity impact (below 3.5km/s) of honeycomb sandwich panels made from PM1000 and PM2000 alloys at elevated temperatures. The impacts have been performed experimentally in a custom gas gun rig, and also by using Finite Element simulations numerically and a phenomenological analytical model. Based on experimental and numerical results we have developed the residual velocity and ballistic limit equations for the test cases. The

developed analytical model is valid when the diameter of the projectile is similar or smaller to the length of the honeycomb cell and the perforation mechanism is dominated by shaped plug formation, causing compression/shear failure in the target. The experimental results and the models proposed provide a general guideline on the effect of the temperature, initial velocity, impact angle and projectile diameter to design thermal protection shields or other high-performance sandwich panels for airframe and spacecraft structures.

Acknowledgements

This work has been supported by the Natural Science Foundation of China (11672088, 11472092, and 11502058), the project supported by the Foundation for Innovative Research Groups of the National Natural Science Foundation of China (No. 11421091), and the National Basic Research Program of China (973 program, No. 2015CB655200).

Reference

[1] Wadley HN. Multifunctional periodic cellular metals. Philosophical Transactions of the Royal Society of London A: Mathematical, Physical and Engineering Sciences. 2006;364(1838):31-68.
[2] Hohe J, Becker W. Effective elastic properties of triangular grid structures. Composite Structures. 1999;45(2):131-45.
[3] Queheillalt DT, Carbajal G, Peterson G, Wadley HN. A multifunctional heat pipe sandwich panel structure. International journal of heat and mass transfer. 2008;51(1):312-26.
[4] Sunami H, Ito E, Tanaka M, Yamamoto S, Shimomura M. Effect of honeycomb film on protein adsorption, cell adhesion and proliferation. Colloids and Surfaces A: Physicochemical and Engineering Aspects. 2006;284:548-51.
[5] Lakes R. Design considerations for materials with negative Poisson's ratios. Journal of Mechanical Design. 1993;115(4):696-700.
[6] Scarpa F, Panayiotou P, Tomlinson G. Numerical and experimental uniaxial loading on in-plane auxetic honeycombs. The Journal of Strain Analysis for Engineering Design. 2000;35(5):383-8.
[7] Zhang Q, Yang X, Li P, Huang G, Feng S, Shen C, et al. Bioinspired engineering of honeycomb structure–Using nature to inspire human innovation. Progress in Materials Science. 2015;74:332-400.
[8] Fleck NA, Qiu X. The damage tolerance of elastic–brittle, two-dimensional isotropic lattices. Journal of the Mechanics and Physics of Solids. 2007;55(3):562-88.
[9] Zhu HX, Mills N. The in-plane non-linear compression of regular honeycombs. International Journal of Solids and Structures. 2000;37(13):1931-49.

[10] Qi C, Yang S, Wang D, Yang L-J. Ballistic Resistance of Honeycomb Sandwich Panels under In-Plane High-Velocity Impact. Scientific World Journal. 2013.
[11] Ebrahimi H, Ghosh R, Mahdi E, Nayeb-Hashemi H, Vaziri A. Honeycomb sandwich panels subjected to combined shock and projectile impact. International Journal of Impact Engineering. 2016;95:1-11.
[12] Wang Z, Tian H, Lu Z, Zhou W. High-speed axial impact of aluminum honeycomb - Experiments and simulations. Composites Part B-Engineering. 2014;56:1-8.
[13] Zhang D, Jiang D, Fei Q, Wu S. Experimental and numerical investigation on indentation and energy absorption of a honeycomb sandwich panel under low-velocity impact. Finite Elements in Analysis and Design. 2016;117:21-30.
[14] Nia AA, Razavi SB, Majzoobi GH. Ballistic limit determination of aluminum honeycombs - Experimental study. Materials Science and Engineering a-Structural Materials Properties Microstructure and Processing. 2008;488(1-2):273-80.
[15] Ryan S, Schaefer F, Riedel W. Numerical simulation of hypervelocity impact on CFRP/Al HC SP spacecraft structures causing penetration and fragment ejection. International journal of impact engineering. 2006;33(1):703-12.
[16] Ryan S, Schaefer F, Destefanis R, Lambert M. A ballistic limit equation for hypervelocity impacts on composite honeycomb sandwich panel satellite structures. Advances in Space Research. 2008;41(7):1152-66.
[17] Ryan S, Schäfer F, Guyot M, Hiermaier S, Lambert M. Characterizing the transient response of CFRP/Al HC spacecraft structures induced by space debris impact at hypervelocity. International Journal of Impact Engineering. 2008;35(12):1756-63.
[18] Morada G, Ouadday R, Vadean A, Boukhili R. Low-velocity impact resistance of ATH/epoxy core sandwich composite panels: Experimental and numerical analyses. Composites Part B: Engineering. 2017;114:418-31.
[19] Liu J, He W, Xie D, Tao B. The effect of impactor shape on the low-velocity impact behavior of hybrid corrugated core sandwich structures. Composites Part B: Engineering. 2017;111:315-31.
[20] Feli S, Pour MHN. An analytical model for composite sandwich panels with honeycomb core subjected to high-velocity impact. Composites Part B-Engineering. 2012;43(5):2439-47.
[21] Buitrago BL, Santiuste C, Sanchez-Saez S, Barbero E, Navarro C. Modelling of composite sandwich structures with honeycomb core subjected to high-velocity impact. Composite Structures. 2010;92(9):2090-6.
[22] Sarasini F, Tirillo J, D'Altilia S, Valente T, Santulli C, Touchard F, et al. Damage tolerance of carbon/flax hybrid composites subjected to low velocity impact. Composites Part B-Engineering. 2016;91:144-53.
[23] Boria S, Santulli C, Sarasini F, Tirillò J, Caruso AP, Infantino M. Potential of wool felts in combination with glass fibres: Mechanical and low velocity impact assessment. Composites Part B: Engineering. 2017;118:158-68.
[24] Scarponi C, Sarasini F, Tirillò J, Lampani L, Valente T, Gaudenzi P. Low-velocity impact behaviour of hemp fibre reinforced bio-based epoxy laminates. Composites Part B: Engineering. 2016;91:162-8.
[25] Zouggar K, Boukhoulda FB, Haddag B, Nouari M. Numerical and experimental investigations of S-Glass/Polyester composite laminate plate under low energy impact. Composites Part B: Engineering. 2016;89:169-86.
[26] Bandaru AK, Ahmad S. Modeling of progressive damage for composites under ballistic impact. Composites Part B: Engineering. 2016;93:75-87.

[27] Xie W, Zhang W, Kuang N, Li D, Huang W, Gao Y, et al. Experimental investigation of normal and oblique impacts on CFRPs by high velocity steel sphere. Composites Part B: Engineering. 2016;99:483-93.
[28] Landowski M, Strugała G, Budzik M, Imielińska K. Impact damage in SiO2 nanoparticle enhanced epoxy – Carbon fibre composites. Composites Part B: Engineering. 2017;113:91-9.
[29] Ravandi M, Teo WS, Tran LQN, Yong MS, Tay TE. Low velocity impact performance of stitched flax/epoxy composite laminates. Composites Part B: Engineering. 2017;117:89-100.
[30] Piekutowski AJ. Characteristics of debris clouds produced by hypervelocity impact of aluminum spheres with thin aluminum plates. International Journal of Impact Engineering. 1993;14(1):573-86.
[31] Piekutowski AJ. Debris clouds produced by the hypervelocity impact of nonspherical projectiles. International journal of impact engineering. 2001;26(1):613-24.
[32] Christiansen EL. Design and performance equations for advanced meteoroid and debris shields. International Journal of Impact Engineering. 1993;14(1):145-56.
[33] Christiansen EL, Kerr JH. Ballistic limit equations for spacecraft shielding. International Journal of Impact Engineering. 2001;26(1):93-104.
[34] Amaro AM, Reis PNB, Neto MA. Experimental study of temperature effects on composite laminates subjected to multi-impacts. Composites Part B: Engineering. 2016;98:23-9.
[35] Liu J, Zhu X, Li T, Zhou Z, Wu L, Ma L. Experimental study on the low velocity impact responses of all-composite pyramidal truss core sandwich panel after high temperature exposure. Composite Structures. 2014;116:670-81.
[36] Walley SM, Field JE, Blair PW, Milford AJ. The effect of temperature on the impact behaviour of glass/polycarbonate laminates. International Journal of Impact Engineering. 2004;30(1):31-53.
[37] Erickson MD, Kallmeyer AR, Kellogg KG. Effect of temperature on the low-velocity impact behavior of composite sandwich panels. Journal of Sandwich Structures and Materials. 2005;7(3):245-64.
[38] Harman A, Rider A. Impact damage tolerance of composite repairs to highly-loaded, high temperature composite structures. Composites Part A: Applied Science and Manufacturing. 2011;42(10):1321-34.
[39] Li T, Mo J, Yu X, Suo T, Li Y. Mechanical behavior of C/SiC composites under hypervelocity impact at different temperatures: Micro-structures, damage and mechanisms. Composites Part A: Applied Science and Manufacturing. 2016;88:19-26.
[40] Salehi-Khojin A, Mahinfalah M, Bashirzadeh R, Freeman B. Temperature effects on Kevlar/hybrid and carbon fiber composite sandwiches under impact loading. Composite Structures. 2007;78(2):197-206.
[41] Halda E, Riney T. Effectiveness of meteoroid bumpers composed of two layers of distinct materials. AIAA Journal. 1968;6(2):338-44.
[42] Lambert M, Schäfer FK, Geyer T. Impact damage on sandwich panels and multi-layer insulation. International Journal of Impact Engineering. 2001;26(1):369-80.
[43] Maiden C, McMillan A. An investigation of the protection afforded a spacecraft by a thin shield. Aiaa Journal. 1964;2(11):1992-8.
[44] Xie W, Meng S, Ding L, Jin H, Han G, Wang L, et al. High velocity impact tests on high temperature carbon carbon composites. Composites Part B: Engineering. 2016;98:30-8.
[45] Schonberg WP. Hypervelocity impact penetration phenomena in aluminum space structures. Journal of Aerospace Engineering. 1990;3(3):173-85.
[46] Schwarzkopf Plansee PM 1000 ODS Nickel Alloy. http://www.matweb.com/search/DataSheet.aspx?MatGUID=38184f5f192a466bb09dadcf803cbd9f&ckck=1: MatWeb; 2016.

[47] Schwarzkopf Plansee PM 2000, Sheet Grain Class 6 ODS Iron Alloy Sheet http://www.matweb.com/search/DataSheet.aspx?MatGUID=21e9ec9a0de24b47bcf69ab11c375567: MatWeb; 2016.
[48] Hayashida K, Robinson J. Double-plate penetration equations. 2000.
[49] Reimerdes H-G, Noelke D, Schäfer F. Modified Cour-Palais/Christiansen damage equations for double-wall structures. International journal of impact engineering. 2006;33(1):645-54.
[50] Ding L, Li C, Pang B, Zhang W. Ballistic limit equations in ballistic and shatter regions. International Journal of Impact Engineering. 2008;35(12):1490-6.
[51] Recht R, Ipson T. Ballistic perforation dynamics. Journal of Applied Mechanics. 1963;30(3):384-90.
[52] Xie ZY. Analytical modeling of plastic response of sandwich constructions under localized indentation and bend [PH.D.]. Hefei: University of Science and Technology of China; 2012.
[53] Watts AJ, Atkinson D. Dimensional scaling for impact cratering and perforation. International journal of impact engineering. 1995;17(4):925-35.